Finite Element Modelling of RC Beams Retrofitted with CFRP Fabrics

by H.B. Pham and R. Al-Mahaidi

Synopsis: In this paper, non-linear finite element modelling of debonding failure of rectangular reinforced-concrete beams strengthened with externally-bonded Carbon Fiber Reinforced Polymer (CFRP) fabrics under bending is presented. Smeared crack models were used to simulate concrete cracking. Interface elements were used to model the bond between concrete and reinforcement. The model proved to be able to simulate the beams' behaviour, predicting the failure modes, the failure loads and the reinforcement strain distributions relatively well. The parametric study using the FEA clarified the effect of several important factors on the capacity of the beams.

499

Huy Binh Pham is a PhD student investigating strengthening concrete structures using FRP.

Riadh Al-Mahaidi is the Head of the Structures Group in the Department of Civil Engineering at Monash University in Melbourne, Australia. He received his MSc and PhD degrees from Cornell University. His research interests include finite element modelling of concrete structures, strength assessment of concrete bridges and rehabilitation of concrete and steel structures using FRP composites. He is a member of ACI-ASCE Committee 447 and ACI-440.

INTRODUCTION

Even for a simply supported rectangular reinforced concrete beam retrofitted with FRP, there is much complication regarding debonding failure. One reason is that the behaviour of those beams is determined by a large number of parameters such as the beam dimensions, the amount of steel reinforcement and the FRP dimensions. As a consequence, even though there have been a large number of experimental studies, the failure mechanisms are still not fully understood and the influences of several parameters are not yet proved clearly.

Nonlinear finite element analysis can provide a powerful tool to study the behaviour of concrete structures. There have been a number of numerical studies of retrofitted beams. Linear elastic analysis has been used to verify the stress concentration at the ends of laminates or at a tip of a flexural crack (Malek et al. 1998; Teng et al. 2002). To be able to pick up the concentration, very fine meshes were required. Non-linear analysis using smeared cracks has been also reported. Two-dimensional models have been built by Arduini et al. (1997), Ross et al. (1999), David et al. (1999), Hearing (2000), Rahimi and Hutchinson (2001) and Yin and Wu (2001). Three-dimensional models were reported in Arduini et al. (1997), Fanning and Kelly (2000), Zarnic and Bosiljkov (2001), Wong et al. (2001) and Shokrieh and Malevajerdy (2001). Most studies were able to predict the overall behaviour of retrofitted beams giving close load versus deflection curves. However, most models were not able to capture local debonding failures. Cracking pattern was rarely reported. Several studies showed the general crack bands but the debond cracks were not observed. There was an attempt to simulate debonding using a new interface element (Wong et al. 2001). However, in this model, delamination surface location was assumed to be the bond line between FRP and concrete with a known interface constitutive relation. In brief, all linear elastic finite element analysis and nonlinear finite element analysis using smeared cracks have not been able to capture clearly debonding failure modes.

In the present study, another attempt was made using non-linear finite element code, DIANA (de Witte and Kikstra, 2003). The tasks are to build a model which can represent the beam crack pattern and predict the ultimate loads reasonably and to use the model to carry out a parametric study.

EXPERIMENTAL STUDY

To investigate the failure mechanisms of RC beams with FRP bonded on soffit, a thorough literature review and an experimental program has been carried out (Pham and Al-Mahaidi, 2004a; Pham and Al-Mahaidi, 2004b). Prediction models have also been proposed (Pham and Al-Mahaidi, 2004c). The experimental program included testing of 18 reinforced concrete beams. The typical beam dimensions material properties are shown in Figure 1 and Table 1. The varied parameters are shown in Table 2.

From these studies, two main flexural debond modes have been identified for retrofitted beams having sufficient shear strength (Figure 2). *End debond* is the failure that originates near the plate end and propagates in the concrete along the tension steel reinforcement. It is the result of the tensile force pulling on the end of FRP. This leads to a high shear stress level at the weakest layer near tension reinforcement level, inducing a longitudinal debonding crack there. *Intermediate span debond* is the failure that originates either from a wide flexural crack (*flexure crack debond*) or a wide flexure shear crack (*flexure-shear crack debond*). It then propagates to the laminate ends parallel to the bonded plate near the adhesive/concrete interface. This debond mode is due to the fact that concrete at the tip of a main flexure-shear crack or flexural crack is subjected to a high tensile force in the CFRP near the crack tip.

FINITE ELEMENT MODELLING

Finite element idealisation

A typical finite element mesh and boundary conditions are shown in Figure 3. The element size was maintained at approximately 12x12 mm. The aspect ratios (length over height) ranged from 1.0 to a 1.2. Since the geometry of the beams, loading and boundary conditions were symmetrical about the centreline, only half a beam was modelled. The model was supported vertically at the base and horizontally at the beam's centreline with roller supports. Load was applied to a single node in the steel plate element.

The concrete was modelled using four-node quadrilateral isoparametric plane stress element (Q8MEM) as shown in Figure 4a. Each element has eight degrees of freedom (dof) with two displacements, u_x and u_y, at each node. A 2 x 2 Gaussian integration scheme was used. The steel and CFRP reinforcement in the beams were modelled as beam element (L7BEN). This is a two-node, two-dimensional beam element. Basic variables are the translations u_x and u_y and the rotation ϕ_z in the nodes (Figure 4b). The element is numerically integrated over their cross-section and along their axis. Two-point and three-point Gauss integration scheme are used along the bar axis and in the bar cross-section respectively. The reinforcement elements are connected to concrete elements by 2+2 nodes structural interface elements (L8IF) as shown in Figure 4c. Three-point Newton-Cotes integration scheme and linear interpolation are used. The nodes for the steel reinforcement were superimposed on top of the concrete nodes.

To avoid stress-locking problem, a rotating crack model was used for the concrete elements below the tension reinforcement. The concrete in this region behaved like plain

concrete. The shear strength of cracked surfaces due to aggregate interlock would be very small and could be ignored. The concrete portion above the tension steel was reinforced with steel bars and should exhibit certain shear strength after cracking. It was modelled with a fixed crack model with a shear retention factor. It was assumed that the shear retention factor was constant. The formulations for these two models are reported in de Witte and Kikstra (2003).

Concrete constitutive relation in tension was described using a nonlinear tension softening stress-strain relationship proposed by Hordijk (1991) and shown in Figure 5a. The peak tensile strength of the concrete was determined accordance to the Comite Euro-International du Beton (1991) (Formula 2.1-4). The area under the stress-strain curve is given by G_f/h, where G_f is the Mode-I fracture energy and h is the crack band width of the element. The crack band width is related to the area of the 2D element, which was determined in DIANA as the square root of the total area of the element. The fracture energy was calculated using the expression by Trunk and Wittmann (1998)

$$G_f = a \cdot d_a^n \tag{1}$$

where d_a is the maximum aggregate size, a = 80.6 and n = 0.32. G_f is in N/mm and d_a is in mm. The shear stiffness of diagonal cracks was assumed to be 5 % of the uncracked concrete.

The behaviour of the concrete in compression is described by the function of Thorenfeldt et al. (1987), which can describe the hardening and softening behaviour of concrete (Figure 5b). More details can be found in de Witte and Kikstra (2003).

The CFRP composite was assumed to be an isotropic material and modelled as linear elastic. The CFRP elastic modulus was taken to be 209000MPa as tested. The Poisson ratio of the CFRP composite was assumed to be 0.30. The adhesive elastic modulus was taken as 8500MPa. A bond-slip relationship, which was established from shear-lap tests (Pham and Al-Mahaidi, 2004d), was assumed for the interface (Figure 5c).

At the tensile reinforcement level, there is reduction of concrete volume due to the presence of the bars. To account for that, the thickness of the concrete at the level of the reinforcement was reduced. This was achieved by reducing the thickness of the concrete elements just below the tensile beam elements such that the concrete area lost was equivalent to the area of tension reinforcement. The influence of concrete area lost associated with compression reinforcement and stirrups was ignored

Verification of finite element model

To verify that the finite element base models simulated the behaviour of the experimental control beam properly, three items from the experimental and numerical results were compared. They were crack patterns at failure, the load displacement behaviour and the strain development in CFRP.

The crack pattern after peak load for the control beam model is illustrated in Figure 6. For clarity, only the cracks, in which the crack strain is large enough so that the crack tensile stress has reduced by 50 % from maximum tensile strength, are shown. The model indicated that the beam experienced main vertical flexural cracks in the constant moment region. It failed by opening of those cracks and crushing of concrete fibre at the top. This is the typical ductile failure of reinforced concrete beams.

For retrofitted beams, the NLFEA indicated two failure modes. The crack pattern developments are illustrated in Figures 7 to 9 for three example beams, E1, S2 and S1, respectively. Failure modes indicated are end span debond, intermediate span debond and a combination of end and intermediate span debond, respectively. The patterns are very similar to those observed in the experiments (Figure 10). Similar results are obtained for all other beams.

The peak loads are compared in Figure 11. The predicted values by FEA agree relatively well with the experimental measurements. The loading curves for E1, S2 and S1 are compared in Figure 12. For S2 and S1 beams, two FE models were built with and without clamping and labelled as 'S2C' and 'S2N', respectively. Again, the predictions and the measurement are in good agreement.

Figure 13 compares the experimental and numerical CFRP strain distributions along the bonded joint for the three beams. The distributions were compared at several load levels. The experimental and numerical load levels were selected to be as close as possible to each other. The distributions match reasonably accurately both for these two examples and for all other beams in the test series as well. Since the debonding failure occurred in a very brittle manner, the experimental CFRP strain distributions during propagation of debonding was not available. Therefore, comparison was not possible after peak.

PARAMETRIC STUDY

Figure 14a plots the predictions of the ultimate shear load capacity for the beam with similar dimension as E1 (E1-type beam) bonded with different CFRP thicknesses. When the FRP thickness is small, the failure mode is intermediate span debond. As the number of plies increases from 1 to 3, the capacity increases to a peak of around 79 kN. As the number of plies increases further, failure modes shifted to end debond and the load capacity reduces relatively.

Figure 14b lists the FEA results for beams with different tensile reinforcement amounts for E1-type beams. Shifting of failure mode from intermediate span debond to end debond (E1-type beams) is also observed as the steel amount increases.

Figure 15 shows the effect of varying CFRP bond length in the shear span. The failure mode is end debond for all cases. As expected, the debonding capacity reduces slightly with the bond length.

CONCLUSIONS

This paper has presented the FEA of a series of retrofitted beams with different parameters. The following findings are drawn from this work:

1) The FE model was able to simulate the beams' behaviour. It predicted the ultimate capacity, the crack patterns as well as the CFRP strain distributions relatively well for all 16 cases. Three failure modes were observed as end debond, intermediate span debond and combination of both end and intermediate span debond.

2) The parametric study was able to clarify the trends as the CFRP thickness, tensile reinforcement amount and CFRP bond length were varied.

REFERENCES

Arduini, M., Di Tommaso, A. and Nanni, A. (1997), "Brittle failure in FRP plate and sheet bonded beams", *ACI Structural Journal*, Vol. 94, No. 4, pp. 363-370.

Comite Euro-International du Beton (1991). CEB-FIP Model Code 1990. London, Great Britain, Thomas Telford.

David, E., Djelal, C., Ragneau, E. and Bodin, F. B. (1999), Use of FRP to strengthen and repair RC beams: experimental study and numerical simulations. Proceedings of the Eighth International Conference on Advanced Composites for Concrete Repair, London, UK.

de Witte, F. C. and Kikstra, W. P. (2003). DIANA User's Manual. Delft, The Netherlands, TNO DIANA BV.

Fanning, P. J. and Kelly, O. (2000), "Smeared crack models of RC beams with externally bonded CFRP plates", *Journal of Computational Mechanics*, Vol. 26, No. 4, pp. 325-332.

Hearing, B. (2000) Delamination in reinforced concrete retrofitted with fiber reinforced plastics. Deparment of Civil and Environmental Engineering, Massachusetts Institute of Technology.

Hordijk, D. A. (1991) Local approach to Fatigue of Concrete, Delft University of Technology.

Malek, A. M., Saadatmanesh, H. and Ehsani, M. R. (1998), "Prediction of failure load of R/C beams strengthened with FRP plate due to stress concentration at the plate end", *ACI Structural Journal*, Vol. 95, No. 2, pp. 142-152.

Pham, H. B. and Al-Mahaidi, R. (2004a), "Assessment of Available Prediction Models for the Strength of FRP Retrofitted RC Beams", *Composite Structures*, Vol. 66, No. 1-4, pp. 601-610.

Pham, H. B. and Al-Mahaidi, R. (2004b), Bonding Characteristics between Fibre Fabrics Bonded to Concrete Members Using Wet Lay-up Method. The Second International Conference on FRP Composites in Civil Engineering, Adelaide, Australia, A. A. Balkema, pp. 407-412.

Pham, H. B. and Al-Mahaidi, R. (2004c), "Experimental Investigation into Flexural Retrofitting of Reinforced Concrete Bridge Beams using FRP Composites", *Composite Structures*, Vol. 66, No. 1-4, pp. 617-625.

Pham, H. B. and Al-Mahaidi, R. (2004d), Predicting models for debonding failures of CFRP retrofitted RC beams. The Second International Conference on FRP Composites in Civil Engineering, Adelaide, Australia, A. A. Balkema, pp. 531-539.

Rahimi, H. and Hutchinson, A. (2001), "Concrete Beams Strengthened with Externally Bonded FRP Plates", *Journal of Composites for Construction*, Vol. 5, No. 1, pp. 44-56.

Ross, C. A., Jerome, D. M., Tedesco, J. W. and Hughes, M. L. (1999), "Strengthening of reinforced concrete beams with externally bonded composite laminates", *ACI Structural Journal*, Vol. 96, No. 2, pp. 212-220.

Shokrieh, M. M. and Malevajerdy, S. A. M. (2001), Strengthening of reinforced concrete beams using composite laminates. FRP composites in civil engineering, Hong Kong, Elsevier, pp. 507-515.

Teng, J. G., Zhang, J. W. and Smith, S. T. (2002), "Interfacial stresses in reinforced concrete beams bonded with a soffit plate: a finite element study", *Construction & Building Materials*, Vol. 16, No., pp. 1-14.

Thorenfeldt, E., Tomaszewicz, A. and Jensen, J. J. (1987), Mechanical properties of high-strength concrete and applications in design. Proc. Symp. Utilization of High-Strength Concrete (Stavanger, Norway), Tapir.

Trunk, B. and Wittmann, F. H. (1998), Experimental investigation into the size dependence of fracture mechanics parameters. Third international conference of fracture mechanics of concrete structures, D-Freiburg: Aedificatio Publ., pp. 1937-1948.

Wong, W. F., Chiew, S. P. and Sun, Q. (2001), Flexural strengthening of RC beams strengthened with FRP plate. FRP composites in civil engineering, Hong Kong, Elsevier, pp. 633-640.

Yin, J. and Wu, Z. (2001), Structural performances of steel-fiber reinforced concrete beams with externally bonded CFRP sheets. FRP composites in civil engineering, Hong Kong, Elsevier, pp. 641-648.

Zarnic, R. and Bosiljkov, V. (2001), Behaviour of Beams Strengthened with FRP and Steel Plates. The 2001 Structural Congress and Exposition, Washington, D.C.

NOTATIONS

a	Shear span
A_f, E_f	Area and Young's modulus of FRP
A_s, E_s	Area and Young's modulus of tension steel
d_a	maximum aggregate size
f_{cm}	mean value of the compressive strength of concrete at the relevant age
f_{ct}	mean value of the tensile strength of concrete
f_{sy}	steel yield stress
G_f	Mode-I fracture energy
L_f	Bonded length of CFRP in shear span

Table 1 - Mechanical properties of materials used

Material	E (MPa)	f_t (MPa)	f_{sy} (MPa)	f_{cm}(MPa)
CFRP fabrics	208000	3800*	-	-
Concrete	-	- - -	-	54 - - -
Steel (Y12)	205000	651	551	-
Steel (Y10)	204000	483	334	-
Steel (Y6)	238000	576	423	-

* given by the manufacturer

Table 2 - Variables in the experimental program

Design	n_s x d_b	$d_{b,sv}$ - s	Cover (mm)	n_f x $t_{f,0}$	L_0 (mm)
Control	3 x 12	10 - 125	25	N/A	N/A
E1	3 x 12	10 - 125	25	6 x 0.176	150
E2	3 x 12	10 - 125	25	6 x 0.176	350
E3	2 x 12	10 - 125	25	6 x 0.176	150
E4	3 x 12	10 - 125	45	6 x 0.176	150
E5	3 x 12	10 - 125	25	9 x 0.176	150
S1	3 x 12	06 - 125	25	2 x 0.176	150
S2	3 x 12	06 - 90	25	2 x 0.176	150
S3	2 x 12	06 - 125	25	2 x 0.176	150

n_s x d_b: number of tension steel bars x bar diameter (mm)
$d_{b,sv}$ - s: stirrup diameters (mm) – spacing (mm)
cover: concrete cover to stirrup
n_f x $t_{f,0}$: number of plies x ply thickness (mm)
L_0: distance from end of FRP to nearest support
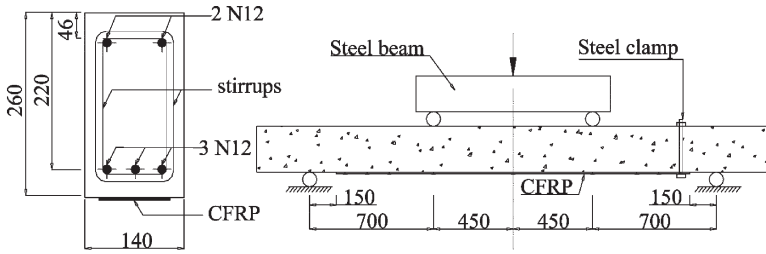
All dimensions are in mm.

Figure 1 - Experiment set-up
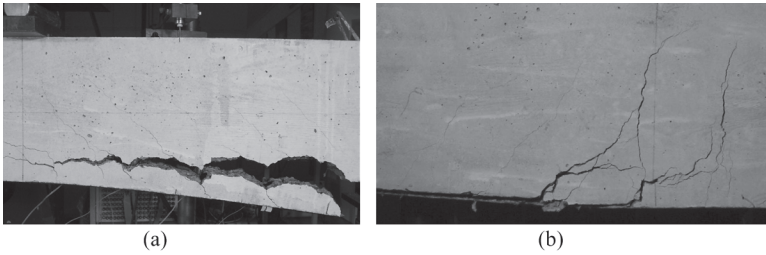
Figure 2 – End cover peeling (a) and mid-span debond (b)
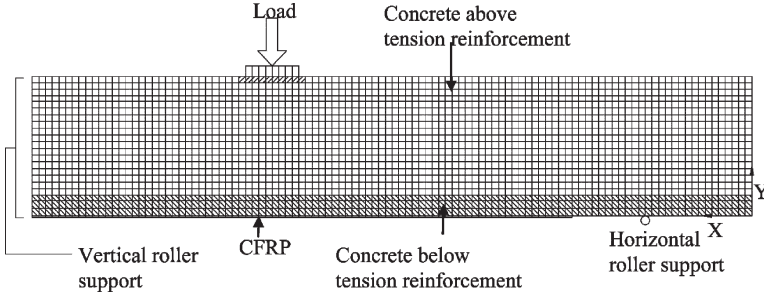
Figure 3 - 2D Mesh of beams loaded in 4-point bending
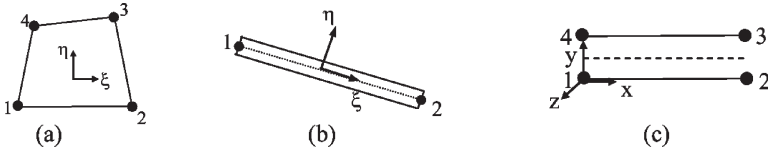
Figure 4 - Q8MEM element (a), L7BEN element (b) and L8IF element (c)

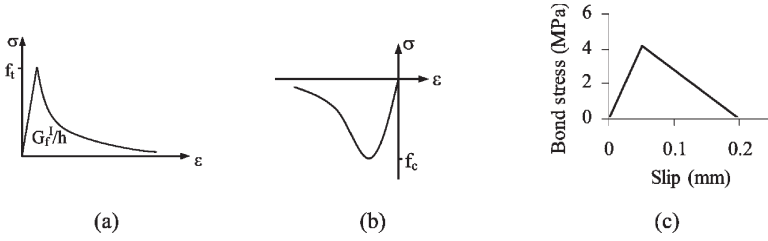(a)   (b)   (c)

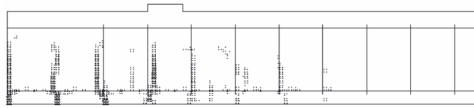Figure 5 - Concrete in tension (a), concrete in compression (b) and
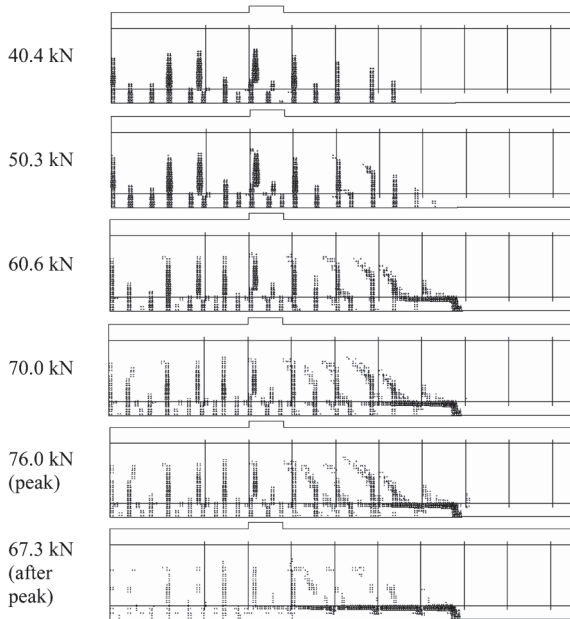interface bond-slip behaviour (c)

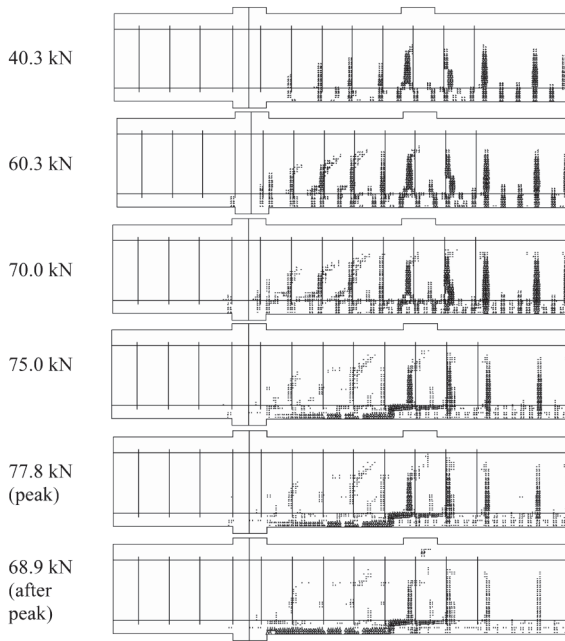Figure 6 – Crack pattern of C1

Figure 7 – Crack pattern development of model E1 (unclamped side)

Figure 8 – Crack pattern development of model S2 (clamped side)
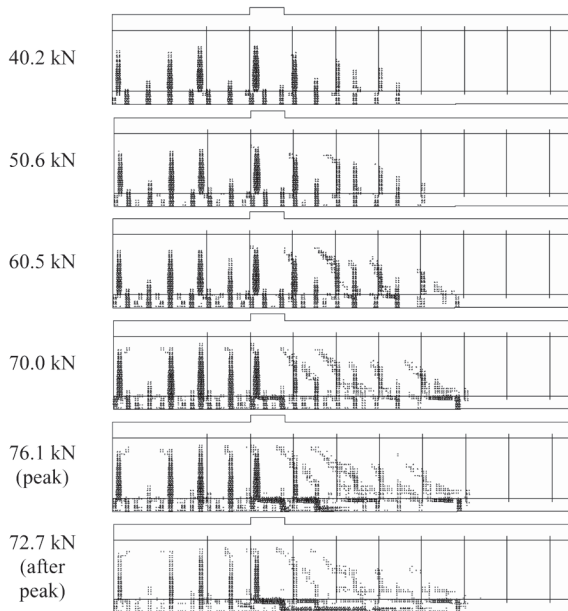
Figure 9 – Crack pattern development of model S1 (unclamped side)

(a)   (b)

(c)
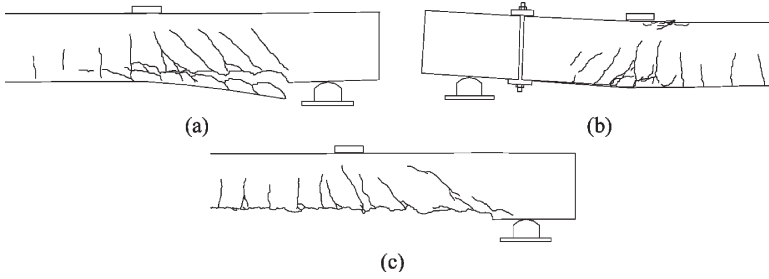
Figure 10 – Observed crack pattern of beams E1 (a), S2 (clamped side) (b) and S1 (unclamped side) (c)
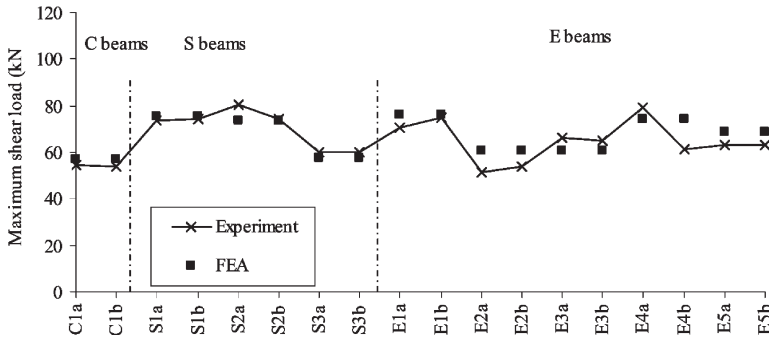
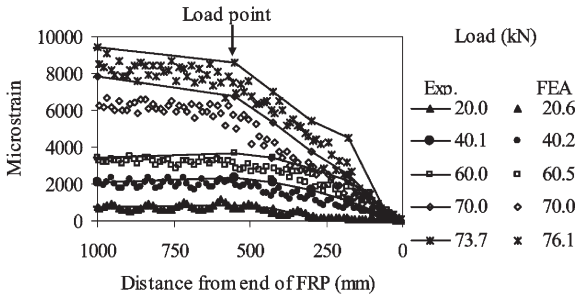Figure 11 – Correlation of peak loads as predicted by the FE model and measured in the experiments

(a)

(b)

(c)
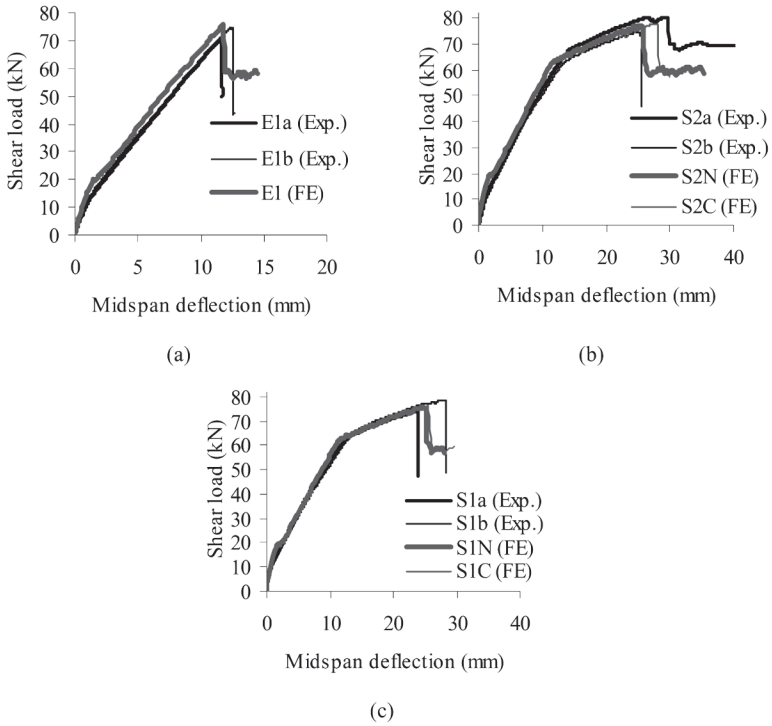
Figure 12 – Comparison of the load-deflection curves for beams E1 (a), S2 (b) and S1 (c)
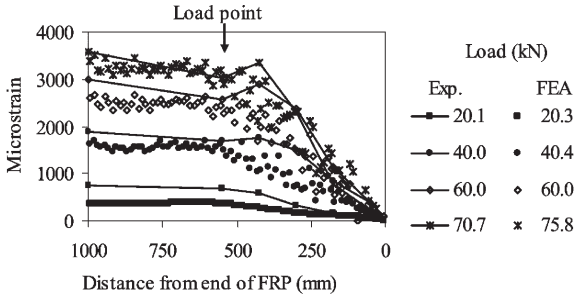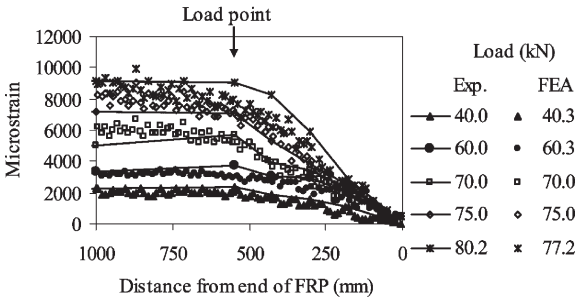
Figure 13 – Comparison of CFRP strain distributions for beams E1a (debonded side) (a), S2a (undebonded side) (b) and S1a (debonded side) (c)
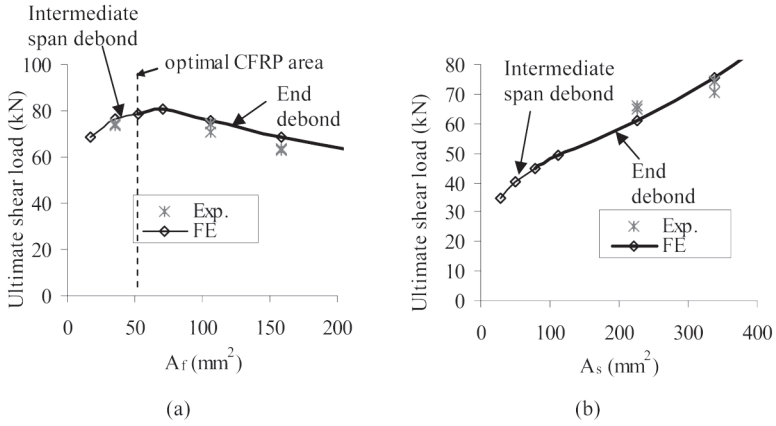
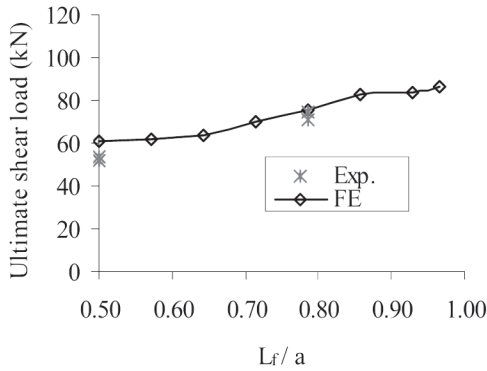Figure 14 – Effect of varying CFRP thickness (a) and tensile reinforcement amount (b)

Figure 15 – Effect of varying CFRP bond length in shear span